Semiclassical analysis of tunnelling splittings in periodically driven quantum systems

1997 J. Phys. A: Math. Gen. 30 1659

(http://iopscience.iop.org/0305-4470/30/5/026)

J. Phys. A: Math. Gen. **30** (1997) 1659–1677. Printed in the UK PII: S0305-4470(97)77025-2

Semiclassical analysis of tunnelling splittings in periodically driven quantum systems

H J Korsch†§, B Mirbach‡ and B Schellhaaß†

† Fachberiech Physik, Universität Kaiserslautern, D-67653 Kaiserslautern, Germany
‡ Facolta die Science, Universitá di Milano, sede di Como, via Lucini 3, I-22100 Como, Italy

Received 8 August 1996, in final form 30 September 1996

Abstract. For periodically driven systems, quantum tunnelling between classical resonant stability islands in phase space separated by invariant KAM curves or chaotic regions manifests itself by oscillatory motion of wavepackets centred on such an island, by mulitplet splittings of the quasienergy spectrum, and by phase space localization of the quasienergy states on symmetry-related flux tubes. Qualitatively different types of classical resonant island formation—due to discrete symmetries of the system—and their quantum implications are analysed by a (uniform) semiclassical theory. The results are illustrated by a numerical study of a driven non-harmonic oscillator.

1. Introduction

The generic phase space structures of classical Hamiltonian systems show an intricate mixture of regular motion on invariant tori and chaotic space filling dynamics. The quantum manifestation of the Poincaré scenario in the statistics of energy spectra, fluctuation of expectation values and wavepacket dynamics is still debated today. An important aspect in this classical-quantum correspondence is the tunnelling dynamics between classical regular regions in phase space divided by separatrices or chaotic layers. Whereas the tunnelling phenomenon is easily understood semiclassically for tunnelling through potential barriers, the general case of *dynamical tunnelling* [1], for example, tunnelling through a classically chaotic region, is far from being fully explored.

The present paper addresses several aspects of a semiclassical analysis of dynamical tunnelling. For simplicity, we will confine our discussion to the case of one-dimensional time-periodic systems, which model, for example, atomic or molecular dynamics in laser fields or driven mesoscopic systems. Such 'one and a half'-dimensional systems show most of the relevant dynamics and allow, on the other hand, extensive numerical studies in the semiclassical regime of small $\hbar$. A considerable number of previous studies on dynamical tunnelling have been carried out for systems of this type, as for instance the studies of a driven double-well oscillator by Lin and Ballentine [2, 3], Peres [4], Plata and Gomez Llorente [5], and Hänggi and co-workers [6–10], the analysis of a generalized kicked rotator [11, 12] or a harmonically driven planar rotor [13] as well as the kicked Harper model [14, 15]. Very recently, the level splitting distribution in chaos-assisted tunnelling two space dimensions has been studied by Leyvraz and Ullmo [16].

§ E-mail address: korsch@physik.uni-kl.de

0305-4470/97/051659+19$19.50

In section 2, we give a brief description of the classical dynamics of the model system. Based on the semiclassical pendulum quantization of KAM resonances derived in a preceding paper [17]—in the following denoted as paper I—a semiclassical analysis of the quasienergy quantization of resonances is presented in section 4. The tunnelling splitting of the quasienergies is discussed in section 5. In particular the structure of the quasienergy spectra, the tunnelling integral over the classical forbidden region and the scaling with $\bar{h}$ are discussed, as well as the differences for the cases of tunnelling between classically connected or disconnected flux tubes. In section 6, the semiclassical dynamics of wavepacket tunnelling between the stability regions is studied.

2. Classical division of phase space

In the present study, we choose as an example the linearly forced anharmonic oscillator

$$H(p,x,t) = \frac{p^2}{2m} + \frac{b}{4}x^4 - \lambda x\cos(\omega t) \tag{1}$$

with units $m = b = \omega = 1$, which is time-periodic with period $T = 2\pi/\omega$.

For $\lambda = 0$, the system reduces to the time-independent (and therefore integrable) quartic oscillator, where a phase space point moves on the energy shell $H(p,x) = E$ with frequency ω_1, which increases with E. For small values of the force amplitude λ, the oscillations in resonance with the driving force, $\omega_1 : \omega = r : s$ with integers r and s, are typically distorted, and a chain of elliptic and hyperbolic fixed points appears. For increasing values of λ, the resonance zones grow and the separatrix dividing the resonance motion from the outer non-resonant oscillation develops into a chaotic layer. Finally, the resonance zones overlap and global chaos sets in. For the parameter $\lambda = \frac{2}{81}\sqrt{3} \approx 0.014\,2556$ (see [18] for the motivation of this special choice) the phase space is predominantly filled by regular motion with isolated resonances, the largest ones at $\omega_1 : \omega = 2:4$, $1:3$, $2:8$, $1:5$ and $1:7$ as shown in the stroboscopic Poincaré section at times $t = nT$, $n = 0, 1, 2, \ldots$, in figure 1.

The Hamiltonian (1) is invariant under the discrete symmetry

$$(p,x,t) \to (\pm p, -x, t + T/2) \tag{2}$$

which appears also in the driven double-well potential (see, e.g. [3, 4]). The dynamical symmetry (2) has important consequences for the phase space organization of the resonant motion. There are two possibilities.

(i) The phase space tube surrounding the periodic orbit at the centre of the resonance is invariant under the symmetry (2). In this case, a Poincaré section of the flux tube at $t = (n + \frac{1}{2})T$ will be a mirror image with respect to $x = 0$ (and $p = 0$) of the Poincaré section at $t = nT$ as, for example, for the 'odd' resonances $1:3$ and $1:5$.

(ii) There are groups of disconnected resonance tubes, each of which violates the symmetry and transforms into another member of this group under the symmetry operation (2). This is a general consequence of the symmetry of the time translation $t \to t + T/2$: it can still be shown that every even resonance chain breaks up into two disconnected ones, where neighbouring islands belong to different chains. A Poincaré section at time $t = (n + \frac{1}{2})T$ will interchange these pairs. In the present case, this is observed for the even $2:4$ and $2:8$ resonance.

The topology of the cable of intertwined flux tubes in (x, p, t) space can be very complicated. Various graphical illustrations of such a cable can be found in the literature (see, e.g. [19, figures 8.3-3] for an outstanding example). Here we will confine ourselves

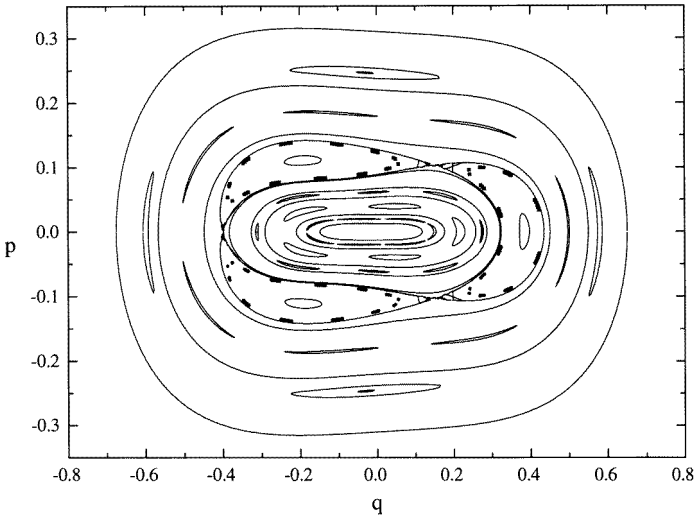

Figure 1. Stroboscopic Poincaré section for a weakly driven quartic oscillator showing resonance regions for $\omega_1/\omega = \frac{1}{2}, \frac{1}{3}, \frac{1}{5}, \ldots$. The period-two motion appears as two disconnected pairs of islands.

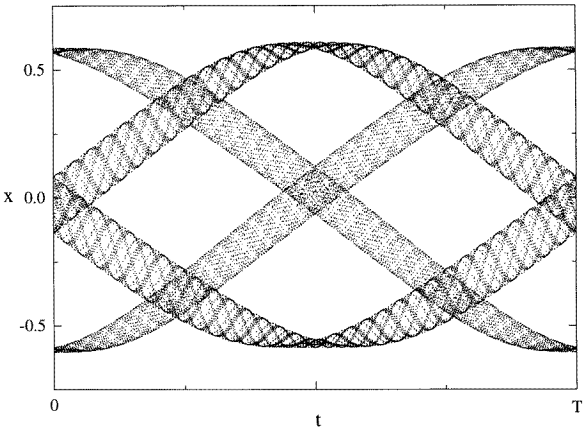

Figure 2. Two pairs of resonant flux tubes surrounding an elliptic orbit of period two. Two different trajectories are plotted as a function of time t modulo $T = 2\pi$.

to the group of flux tubes of single isolated resonances, as illustrated in paper I in (x, p, t) space. Figure 2 shows as an example the projection of such a group of flux tubes on the (x, t) plane for the 2 : 4 resonance. As discussed in (ii) above, we see two pairs of disconnected tubes. Quantum mechanically, these four segments of tubes will lead to four (almost degenerate) quasienergy states, as discussed in detail in the following sections.

Table 1 lists the important parameters of the classical resonance dynamics, the area A_- enclosed by the largest invariant non-resonant curve *below* the resonance, the area A_+ enclosed by the smallest invariant non-resonant curve *above* the resonance and the resonance area $A = A_+ - A_-$. The average of the areas A_+ and A_- determines approximately the

Table 1. Parameters of some classical $r : s$ resonances

$r : s$	A_-	A_+	A	$\omega_0 T$	$S_{\rm po}^+$
1 : 1	3.097 80	5.090 07	1.991 86	0.064 48	1.066 92
2 : 4	0.485 28	0.528 51	0.043 23	0.014 26	0.126 21
1 : 3	0.110 96	0.192 11	0.081 15	0.072 19	0.038 78
1 : 5	0.028 37	0.036 10	0.007 54	0.031 81	0.006 49
2 : 5	0.867 80	0.883 54	0.015 24	0.006 94	0.655 24
1 : 7	0.011 12	0.012 16	0.000 88	0.010 69	0.000 64
2 : 7	0.315 98	0.322 70	0.006 60	0.008 13	0.236 89
1 : 9	0.005 34	0.005 53	0.000 00	0.003 14	0.000 00

average action-variable $I = \oint p\,\mathrm{d}x/2\pi$ of the resonance zone

$$I_{1,0} = \frac{1}{4\pi}(A_+ + A_-). \tag{3}$$

In addition, the eigenvalues of the stability matrix $\mathrm{e}^{\pm \mathrm{i}\omega_0 T}$ at the stable fixed point are needed in the following, as well as the action integral $S_{\rm po}^+$ along the s-periodic orbit at the fixed point.

In the following, we will analyse in detail the dynamics of the 1 : 3 resonance centred at the periodic orbit started at, for example, $(p, x) = (0, 0.385)$ and the 2 : 4 resonances, i.e. the symmetry-related pair of two-periodic orbits started at, for example, $(p, x) = (0, -0.600)$ or $(0.246, -0.027)$, respectively (compare with figure 2).

3. Quantum quasienergies and scaling properties

The quantum dynamics of a time (T)-periodic system can be conveniently described in terms of the quasienergy (Floquet) states

$$\Psi_\nu(t) = \mathrm{e}^{-\frac{\mathrm{i}}{\hbar}\varepsilon_\nu t} u_\nu(t) \qquad \text{with } u_\nu(t+T) = u_\nu(t) \tag{4}$$

which closely resemble the eigenstates of time-independent systems. The quasienergies ε_ν are only defined by (4) up to integer multiples of $\hbar\omega(\omega = 2\pi/T)$. It is therefore convenient to define the quasiangles

$$\theta_n u = \varepsilon_\nu T/\hbar. \tag{5}$$

For Hamilitonian (1), the quasienergy spectrum is a pure point spectrum [20].

The time-periodic Schrödinger equation

$$\mathrm{i}\hbar\frac{\partial\psi}{\partial t} = -\frac{\hbar^2}{2m}\frac{\partial^2\psi}{\partial x^2} + \left(\frac{b}{4}x^4 - \lambda x\cos(\omega t)\right)\psi \tag{6}$$

can be simplified by scaling the variables and parameters as

$$t' = \omega t \qquad x' = x\frac{b^{1/2}}{\omega m^{1/2}} \qquad \lambda' = \lambda\frac{b^{1/2}}{\omega^3 m^{3/2}} \qquad \hbar' = \hbar\frac{b}{\omega^3 m^2} \tag{7}$$

which transforms (6) into

$$\mathrm{i}\hbar'\frac{\partial\psi}{\partial t} = -\frac{\hbar^2}{2}\frac{\partial^2\psi}{\partial x^2} + \left(\frac{1}{4}x^4 - \lambda' x\cos t\right)\psi. \tag{8}$$

The quasienergies scale as

$$\varepsilon' = \varepsilon\frac{b}{\omega^4 m^2} \tag{9}$$

and the quasiangles are, of course, independent of the scaling.

Here we will use the scaled quantities (dropping the prime in the following sections). In the classical limit, the dynamics depends only on a single parameter, λ', and the (scaled) Planck constant, $\bar{h}'$, of the quantum dynamics can be controlled by changing the frequency, ω.

4. Pendulum quantization and semiclassical analysis

Semiclassical EBK quantization techniques for the quasienergy states for time-periodic systems have been developed and studied recently [21, 22]. They allow a quantization in two independent steps, in contrast to related methods for general two-dimensional systems (see, e.g. [23, ch 7.3] and references therein).

For a non-resonant motion, the first quantization step determines the classical torus with quantized action

$$I_1 = \frac{1}{2\pi}\oint_{\gamma_1} p\,\mathrm{d}x = \bar{h}\left(n_1 + \frac{\mu_1}{4}\right) \qquad n_1 = 0,\ 1,\ \ldots \tag{10}$$

where γ_1 is a closed path following the intersection of the torus with the stroboscopic Poincaré section and μ_1 is the Maslov index of the path (e.g. $\mu_1 = 2$ for a liberational motion with two turning points). The subsequent step simply determines the quasienergies

$$\varepsilon_{n_1,n_2} = \omega_1\left(n_1 + \frac{\mu_1}{4}\right) - \langle L\rangle + \bar{h}\omega n_2 \tag{11}$$

in terms of the torus average or, equivalently, the long-time average of the Lagrangian

$$\langle L\rangle = \lim_{k\to\infty}\frac{1}{kT}\int_0^{kT} L(x,\dot{x},t)\mathrm{d}t. \tag{12}$$

The frequency ω_1 in (11) is the angular frequency corresponding to the action I_1. It should be noted that the quantum mechanical quasienergies are only determined up to multiples of $\bar{h}\omega$, and the term $\bar{h}\omega n_2$ in (11) is irrelevant.

Due to the phase space organization in the one-dimensional case, the quantization condition (10), which labels the torus supporting the quasienergy state n_1, also counts the number of states supported by the phase space region *enclosed* by the curve γ_1, which is given by

$$n_1 + 1 = \frac{1}{h}(\text{area enclosed by } \gamma_1) + \frac{\mu_1}{4}. \tag{13}$$

We therefore expect (for $\mu_1 = 2$) $N_+ = A_+/h + \frac{1}{2}$ states supported by the phase space region inside the quantized invariant torus above the resonance (state $n_1^+ = N_+ - 1$) and $N_- = A_-/h + \frac{1}{2}$ states below the resonance region, i.e. the quasienergy state with quantum number $n_1^- = N_- - 1$ is the highest state below. The $N_+ - N_- = A/h$ resonance states must be labelled in a different manner. For the value $\bar{h} = 0.0005$ we have $N = A/h \approx 26$ states localized on the 1 : 3 resonance islands chain and $N = A/h \approx 14$ states on the four 2 : 4 resonance islands.

In comparison with exact results, the semiclassical quantization of non-resonant tori, i.e. tori outside the resonance zones, proved to yield very good results as demonstrated in paper I. Even in cases close to resonances, where the quantizing tori are already destroyed and chaotic layers exist, interpolation techniques yield good approximations to the quasienergies, as long as the resonances zones are small compared with Planck's constant [22]. In paper I, the semiclassical quantization of the KAM resonances, and in particular

the case of large resonances supporting several quantum states, has been addressed in more detail. At resonance, i.e. for a rational frequency ratio $\omega_1 : \omega = r : s (r, s \in \mathbb{N}$, the relevant dynamics is described by a pendulum (see [24] for a related pendulum approximation applied to periodically driven hydrogen atoms). The wavefunctions, $\Phi(\varphi)$, for this pendulum satisfy the Mathieu differential equation

$$\left(\frac{\mathrm{d}^2}{\mathrm{d}\varphi^2} + a - 2q\cos(s\varphi)\right)\Phi(\varphi) = 0 \tag{14}$$

where φ is the pendulum angle.

In the classical limit, the pendulum motion can execute librational (for $a > 2q$) or rotational (for $a < 2q$) motion in different regions in phase space divided by the separatrix ($a = 2q$). The area enclosed by the separatrix is $16\sqrt{q}$, which must be mapped onto the classical resonance area A divided by $\overline{h}$ (compare with section 2). This determines the Mathieu parameter

$$q = (A/16\overline{h})^2. \tag{15}$$

The boundary conditions for the solutions of (14) are

$$\Phi_l\left(\varphi + \frac{2\pi}{s}\right) = \exp\left(\mathrm{i}\frac{2\pi}{s}\left(l + \frac{\mu}{4}\right)\right)\Phi_l(\varphi) \qquad l = 0, \ldots, s-1 \tag{16}$$

where the 'Maslov index' μ is determined by

$$\frac{\mu}{4} = \left(\frac{\mu_1}{4} - \frac{1}{\overline{h}}I_{1,0}\right) \bmod s \tag{17}$$

(note the wrong sign in equation (48) of paper I). Here, $I_{1,0}$ is the location of the resonance, which is given by the average action (3). It should be noted that the Maslov index μ is real valued, i.e. *not* equal to an integer.

As well known from the theory of the Mathieu equation, the boundary condition (16) determines (for any value of l) a characteristic value of a inside the stability bands numbered by $j = 0, 1, \ldots$, i.e. one obtains the characteristic values $a_{j,l}$, which finally map onto the quasienergies by

$$\varepsilon_{j,l,n_2} = \varepsilon'_{j,l} + \overline{h}\omega\left(n_2 + \frac{r}{s}l\right) \tag{18}$$

with

$$\varepsilon'_{j,l} = -\frac{1}{sT}S^+_{\mathrm{po}} + \frac{\overline{h}\omega_0}{2s\sqrt{q}}(a_{j,l} + 2q) + \overline{h}\omega\frac{\mu_1 r}{4s}. \tag{19}$$

The quasienergies ε_{j,l,n_2} taken modulo $\overline{h}\omega/s$ agree with the $\varepsilon'_{j,l}$.

Let us recall from paper I that S^+_{po} is the classical action along the s-periodic orbit centred at the elliptic fixed point and ω_0 is the characteristic frequency for the motion close to the fixed point determined by the eigenvalues of the stability matrix. As discussed in detail in paper I, an expression equivalent to (19) can be derived using data from the hyperbolic fixed points.

In the following, the structural organization of the semiclassical resonance spectrum is analysed. Quite conveniently, we will use the solid-state term 'band' to describe a set of quasidegenerate levels (modulo $\overline{h}\omega(n_2 + r/s)$) belonging to symmetry-related flux tubes.

In paper I, a detailed comparison of exact quantum results demonstrated the quality of the semiclassical pendulum quantization for resonances as well as the semiclassical assignment of quantum numbers, which reveals the underlying structure of the spectrum. In particular, the quasienergies of states localizing on a $r : s$ resonance appear as s-multiplets, which are

almost degenerate if they are taken modulo $\hbar\omega/s$. The presented uniform method provided already quasienergy splittings due to tunnelling. The characteristic values of the Mathieu equation (14) were determined numerically in paper I.

It is, however, more informative in the present context of a semiclassical approximation to treat also the quantization of the Mathieu equation semiclassically. A uniform semiclassical solution of the one-dimensional time-periodic Schrödinger equation is known and explored in particular in the Mathieu case. Here we follow the treatment by Connor *et al* [25]. The semiclassical quantization condition for the solution of the Mathieu equation (14) with boundary condition (16) reads

$$\cos(\alpha-\phi)=[1+\exp(-2\pi\epsilon)]^{-1/2}f_l \qquad \ell=0,\ldots,s-1 \tag{20}$$

where the factors

$$f_l=\cos\frac{2\pi}{s}\left(l+\frac{\mu}{4}\right) \tag{21}$$

satisfy the sum rule $\sum f_l=0$. Here,

$$\alpha=\int_{\varphi_-}^{\varphi_+}\sqrt{a-2q\cos(s\varphi)}\,\mathrm{d}\varphi \tag{22}$$

is the action integral over the well and

$$\pi\epsilon=\pm\int_{\varphi_-}^{\varphi_+}\left|\sqrt{a-2q\cos(s\varphi)}\right|\mathrm{d}\varphi \tag{23}$$

is the tunnelling integral over the forbidden region (the 'barrier'). The boundaries of integration are the zeros of the integrand (the 'classical turning points'), which are real valued for $a\leqslant 2q$ and complex for $a>2q$. The sign in (23) is chosen so that ϵ is negative below and positive above the barrier at $a=2q$.

Because of the phase correction term

$$\phi(\epsilon)=\epsilon+\arg\Gamma\left(\tfrac{1}{2}+\mathrm{i}\epsilon\right)-\epsilon\ln|\epsilon|=-\phi(-\epsilon) \tag{24}$$

the semiclassical formula is valid uniformly below and above the barrier. For the Mathieu case, the phase integrals can be expressed by

$$\alpha=\sqrt{q}\frac{8}{s}\begin{cases}\mathrm{E}(k)-k'^2\mathrm{K}(k) & a\leqslant 2q\\ k\mathrm{E}(k^{-1}) & a>2q\end{cases} \tag{25}$$

$$\pi\epsilon=\sqrt{q}\frac{8}{s}\begin{cases}\mathrm{E}(k')-k^2\mathrm{K}(k') & a\leqslant 2q\\ \mathrm{K}(|k'|/k)-\mathrm{E}(|k'|/k) & a>2q\end{cases} \tag{26}$$

in terms of elliptic integrals $\mathrm{E}(k)$ and $\mathrm{K}(k)$ with $k^2=(a+2q)/4q$ and $k'^2=1-k^2$ following the notation in [26]. At the separatrix $a=2q$ we have

$$\alpha_{\mathrm{sep}}=\frac{8}{s}\sqrt{q} \qquad \text{and} \qquad \epsilon=\phi=0 \tag{27}$$

Equation (20) can be rewritten [25] as

$$\alpha-\phi=\pi(j+\tfrac{1}{2})-(-1)^j\arctan\frac{f_l}{\sqrt{1-f_l^2+\exp(-2\pi\epsilon)}} \tag{28}$$

where $j=0,1,\ldots$ counts the consecutive multiplicities of the arctan function and determines the 'band number'.

The numerical solution of (20) or (28) determines the uniform semiclassical characteristic values $a_{j,l}$ of the Mathieu equation for boundary condition (16). Figure 3

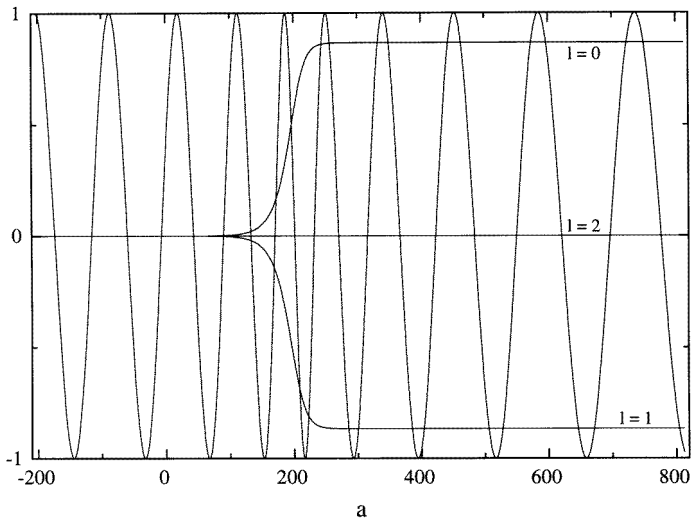

Figure 3. Semiclassical quantization condition (20) as a function of the Mathieu parameter a for a period three ($s = 3$) chain in figure 1 ($\bar{h} = 0.0005$). The three branches of the right-hand side differ by the factor f_l, $l = 0, 1, 2$.

illustrates this for the case of a three-island chain ($s = 3$) and parameter $q = 101.7$ (adapted to the period-three chain of resonances shown in figure 1), Maslov index $\mu \approx 1$ and $\omega_0 = 0.071\,29$. Both sides of the equality (20) are shown separately as a function of a (note that the right-hand side leads to three branches $l = 0, 1, 2$ because of the factor f_l). In figure 3, we have $f_2 \approx 0$, $f_0 = 0.867$, and $f_1 = -0.867$ (note that for different parameters these values are different, in particular we have $f_2 \neq 0$ and $f_0 \neq -f_1$ as demonstrated numerically below). The right-hand side of (20) changes continuously from zero to a plateau, f_l, with a steep increase in the vicinity of $a = 2q$ at the separatrix, where the tunnelling integral is zero. The intersections of the curves determine the characteristic values $a_{j,l}$. For the eight bands $j = 0, 1, \ldots 7$ inside the separatrix at $a_{\text{sep}} = 2q \approx 203$, the splittings of the a-values are small.

The numerical results for the quasiangles for the 1 : 3 resonance states are listed in table 2, where the quasiangles θ' are taken modulo $2\pi/3$. The θ' appear as almost degenerate triples, which are clearly organized in bands numbered by j. A first assignment of the semiclassical quantum numbers $l = 0, 1, 2$ is supported by the shifts $\pi l/3$ of the θ-triple before the modulo operation. Also shown in the table are the present semiclassical quasienergies (column scl(2)) obtained from (19), which are in very good agreement with the more elaborate ones given in paper I (listed in column scl(1)). (Note that the l numbering in paper I differs from the present one.) Furthermore, one observes that the triple of quasiangles for $l = 0, 1, 2$ changes its order for odd or even values of the band number j, which is easily explained semiclassically because of the alternating sign of the slope of the cos function in figure 3. Interestingly, the semiclassical quasienergy splittings yield good approximations to the exact splittings even for states localizing definitely outside the resonance, i.e. $j > 8$. There the underlying pendulum approximation loses its legitimation, and the absolute values of the semiclassical quasienergies increasingly deviate from quantum values. The noticeable deviation between the semiclassical and the quantum values for the extremely small splittings in the lowest bands, however, are due to the limited accuracy in the quantum computations.

Table 2. Semiclassical and exact quantum quasiangles $\theta'_{jl} = \varepsilon'_{jl}T/\hbar$ (modulo $2\pi/3$) for the 1 : 3 resonance states. The quantum numbers (j, l) are assigned semiclassically. The exact quantum results are compared with the semiclassical approximation scl(2) and with those obtained from the more elaborate method in paper I (scl(1)).

		Quasiangles			Energy splittings		
j	l	Quantum	scl(1)	scl(2)	Quantum	scl(1)	scl(2)
0	0	0.5467	0.5458	0.5472			
0	1	0.5467	0.5458	0.5472	1.49e − 09	1.31e − 11	1.68e − 11
0	2	0.5467	0.5458	0.5472			
1	0	0.9816	0.9818	0.9832			
1	1	0.9816	0.9818	0.9832	3.82e − 09	1.28e − 09	1.24e − 09
1	2	0.9816	0.9818	0.9832			
2	0	1.3969	1.3993	1.4007			
2	1	1.3969	1.3993	1.4007	2.55e − 08	5.79e − 08	1.24e − 08
2	2	1.3969	1.3993	1.4007			
3	0	1.7913	1.7967	1.7981			
3	1	1.7913	1.7967	1.7981	1.30e − 06	1.61e − 06	1.59e − 06
3	2	1.7913	1.7967	1.7981			
4	0	0.0683	0.0776	0.0790			
4	1	0.0683	0.0776	0.0790	2.56e − 05	3.07e − 05	3.04e − 05
4	2	0.0683	0.0776	0.0790			
5	0	0.4144	0.4284	0.4298			
5	1	0.4140	0.4280	0.4294	3.29e − 04	4.16e − 04	4.13e − 04
5	2	0.4144	0.4282	0.4296			
6	0	0.7290	0.7475	0.7490			
6	1	0.7325	0.7515	0.7530	3.52e − 03	4.01e − 03	3.99e − 03
6	2	0.7296	0.7494	0.7509			
7	0	1.0194	1.0460	1.0475			
7	1	0.9954	1.0203	1.0219	2.39e − 02	2.57e − 02	2.56e − 02
7	2	1.0099	1.0321	1.0337			
8	0	1.1995	1.2279	1.2296			
8	1	1.2836	1.3162	1.3177	8.41e − 02	8.83e − 02	8.81e − 02
8	2	1.2333	1.2639	1.2656			
9	0	1.5619	1.5822	1.5837			
9	1	1.3904	1.4194	1.4210	1.72e − 01	1.63e − 01	1.63e − 01
9	2	1.4477	1.4941	1.4956			
10	0	1.1674	1.6802	1.6816			
10	1	1.8068	1.8903	1.8916	1.89e − 01	2.10e − 01	2.10e − 01
10	2	1.7744	1.7820	1.7834			
11	0	0.1430	0.1497	0.1509			
11	1	2.0121	2.0032	2.0045	1.87e + 00	1.98e + 00	1.98e + 00
11	2	2.0144	0.0272	0.0285			
12	0	0.1796	0.2774	0.2786			
12	1	0.4647	0.5454	0.5466	2.85e − 01	2.68e − 01	2.68e − 01
12	2	0.3803	0.4089	0.4101			
13	0	0.8951	0.9790	0.9801			
13	1	0.6312	0.6855	0.6867	2.64e − 01	2.93e − 01	2.93e − 01
13	2	0.7726	0.8305	0.8316			

Figure 4 shows the quasiangles θ_j for the 1 : 3 resonance states taken modulo $2\pi/3$ as a function of the band number j (compare with figure 6 of paper I). The quasiangles (modulo $2\pi/3$) appear as almost degenerate triples, where the splitting increases with j, as discussed in detail in the following section. For the average value $\bar{f} = \sum_l f_l/s = 0$ we

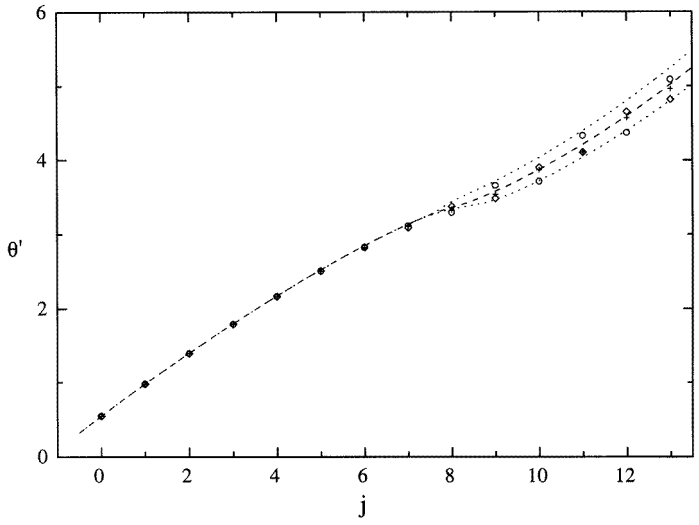

Figure 4. Quaisangles θ' (modulo $2\pi/3$) for the 1 : 3 resonance states as a function of the band number j (integer multiples of $2\pi/3$ are added so that the data increase with j). The almost degenerate triples for $l = (\bigcirc)$, $1(\diamondsuit)$, and $2(+)$ changes its order for odd and even j. The broken and dotted curves show the variation of the semiclassical band centre and band boundaries.

have (compare with (28))

$$\alpha - \phi = \pi\left(j + \tfrac{1}{2}\right) \tag{29}$$

which determines the band centre $\bar{a}_j$ as a function of j. More directly, the inverse function is explicitly given as

$$\bar{j} = \frac{1}{\pi}(\alpha - \phi) - \frac{1}{2} \tag{30}$$

where α and ϕ are given in (22) and (24) as a function of the parameter a, which can be determined from (19):

$$a(\theta') = \frac{2s\sqrt{q}}{\omega_0 T}\left(\theta' + \frac{S_{\mathrm{po}}^{+}}{s\bar{h}} - 2\pi\frac{\mu_1 r}{4s}\right) - 2q. \tag{31}$$

Therefore, (30) provides the typical dependence of the band centre as a function of the quasiangle θ' valid uniformaly across the separatrix. Similarly, the semiclassical band edges can be determined from (28) using the extreme case $f_\ell = \pm 1$. This leads to

$$j_\pm = \bar{j} \pm \arctan(\exp(\pi\epsilon)) \tag{32}$$

which increases with ϵ from zero below the separatrix to $\bar{j} \pm \frac{1}{2}$, i.e. the j band width approaches unity.

Both, the band centre and the upper and lower band edges are also shown in figure 4 as broken or dotted curves, respectively. We observe a marked change of the slope close to the separatrix band number estimated as

$$j_{\mathrm{sep}} = A/sh - \tfrac{1}{2} \tag{33}$$

which yields $j_{\mathrm{sep}} = 8.06$ in agreement with figure 4. For larger band numbers, the triple of exact quantum values follow the semiclassical boundaries. Finally, it should be noted that well below the barrier $-\pi\epsilon$ is very large in the semiclassical limit and the tunnelling

contribution in (28) can be neglected ($\phi = 0$) and we recover the primitive semiclassical quantization (see paper I)

$$\alpha = \pi\left(j + \tfrac{1}{2}\right) \tag{34}$$

in agreement, of course, with the band centre (29) for $\phi = 0$. In this limit, $\varepsilon'_{j,l}$ in (19) is l-independent

$$\varepsilon'_{j,l} \approx \overline{\varepsilon'_j} = -\frac{1}{sT}S^+_{\mathrm{po}} + \frac{\hbar\omega_0}{2s\sqrt{q}}(\bar{a}_j + 2q) + \hbar\omega\frac{\mu_1 r}{4s}. \tag{35}$$

Even more drastically, the elliptic functions in (26) can be expanded to first order in k^2 and one obtains

$$\overline{\varepsilon'_j} \approx -\frac{1}{sT}S^+_{\mathrm{po}} + \hbar\omega_0\left(j - \frac{1}{2}\right) + \hbar\omega\frac{\mu_1 r}{4s} \tag{36}$$

i.e. a contribution from the central periodic orbit and an additive harmonic oscillator ladder from the harmonically approximated pendulum. Formula (36) can also be obtained from the torus quantization by expanding expression (11) to the first order in the action I_1, which agrees with the narrow approximation by Bensch and Thylwe [27] for the case of a single flux tube.

The localization properties of states related to the 1 : 3 resonance are most clearly detected in the quantum phase space densities, as for instance the Husimi density

$$\varrho(p, x) = |\langle p, x|\Psi\rangle|^2 \tag{37}$$

which is simply the projection on minimum uncertainty states localized at point (p, x) in phase space:

$$\langle y|p, x\rangle = \left(\frac{s}{\pi\hbar}\right)^{1/4}\exp\left(-\frac{s(y-x)^2}{2\hbar} + \frac{\mathrm{i}}{\hbar}py\right). \tag{38}$$

Figure 5 shows the Husimi distribution for a number of selected states computed from the exact quantum states. As in paper I, the exact quasienergy states are ordered according to increasing expectation values $\langle\alpha|\hat{H}(t = 0)|\alpha\rangle$. Here we use an index, γ, to number the states in this way. In addition, the semiclassically assigned quantum numbers (j, l) are given. As expected, states with $j < 8$ localize on the stability islands, as shown for the lowest states (the resonance 'ground states') $j = 0$ and the excited states $j = 3$. With increasing j, the Husimi distributions show an increasing number of maxima, but—for low j—the distributions for the three l substates are almost identical. This changes, however, the vicinity of the separatrix. The three 'separatrix states' with $j = 8$ show a pronounced localization in the vicinity of the hyperbolic fixed points, where two maxima are observed close to these unstable fixed points. States $(j, l) = (8, 0)$ and (8, 1) localize predominantly on the outer, whereas state $(j, l) = (8, 2)$ localizes on the inner branch of the separatrix. The states in the next higher band, $j = 9$, also populate the hyperbolic fixed points, however, clearly outside the classical separatrix (state $(j, l) = (9, 2)$ is shown as an example) and, consequently, these states can be quantized also by primitive EBK torus quantization on a torus outside the separatrix (see paper I).

As an example of the organization of quasienergies for an even resonance, the $r : s = 2 : 4$ resonance will be discussed in some detail. As already pointed out in section 2, an even resonance breaks up to two disconnected subchains, i.e. we observe a chain of four two-periodic islands in the classical Poincaré section in figure 1, where the pairs of opposite islands are connected by a flux tube. As shown in figure 2, the two pairs of disconnected flux tubes interchange their position each half period, $T/2$. Therefore, after

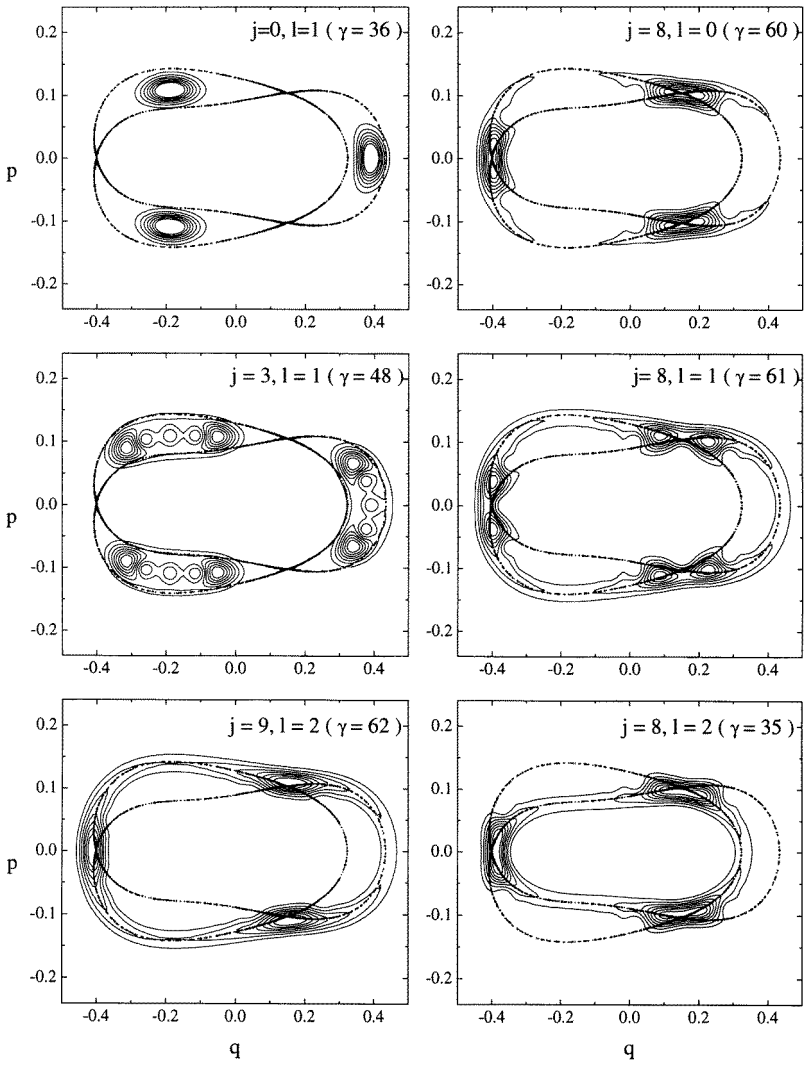

Figure 5. Quantum Husimi phase space distributions for a number of selected states with semiclassically assigned quantum number (j, l) related to the 1 : 3 resonance. States with $j < 8$ localize on the stability islands, as shown for the lowest states (the resonance 'ground state') $j = 0$ and the excited states $j = 3$. The states $j = 8$ localize on the separatrix and $j = 9$ in the region outside the separatrix.

one period T, each pair of flux tubes is at its starting position; however, the position of the flux tubes within such a pair is restored only after $2T$.

The total resonance area is $A = 0.043\,23$ and we expect 14 states localized inside the resonance islands. The semiclassical parameter q is therefore equal to 29.187 and the separatrix band (33) is expected at $j_{\mathrm{sep}} \approx 2.9$. Furthermore, we have a Maslov index $\mu = 12.608$. A semiclassical quantization of such an island chain has been derived in section 6 of paper I, which leads to the simple semiclassical quantization of each of the two-periodic flux tubes as discussed above. This yields two sets of quasiangles, which are degenerate modulo $2\pi/s = \pi$.

Table 3. Semiclassical (first line, scl) and exact quantum (second line, qm) quasiangles $\theta'_{jl} = \varepsilon'_{j,l}T/\hbar$ (modulo $2\pi/2$) for the 2 : 4 resonance states. The quantum numbers (j, l) are assigned semiclassically.

j		$l = 0$	$l = 1$	$l = 2$	$l = 3$
0	scl	1.0974	1.0975	1.0975	1.0975
	qm	1.0958	1.0958	1.0958	1.0958
1	scl	1.2236	1.2240	1.2234	1.2231
	qm	1.2218	1.2221	1.2216	1.2212
2	scl	1.3298	1.3266	1.3321	1.3363
	qm	1.3281	1.3244	1.3296	1.3344
3	scl	1.4189	1.4411	1.4101	1.3986
	qm	1.4141	1.4403	1.4099	1.3959
4	scl	1.4959	1.4658	1.5119	1.5517
	qm	1.4984	1.4616	1.5041	1.5554
5	scl	1.6371	1.6877	1.6161	1.5707
	qm	1.6258	1.6953	1.6218	1.5615

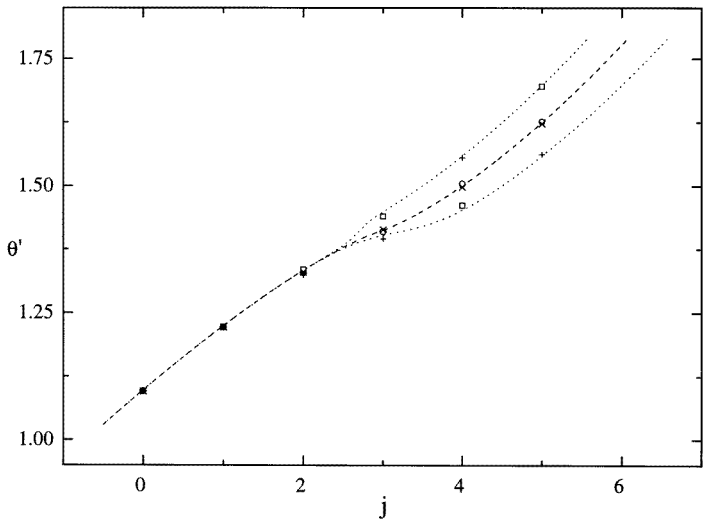

Figure 6. Quasiangles θ' (modulo $2\pi/2$) for the 2 : 4 resonance states as a function of the band number j. The almost degenerate pair for $l = 0, 2$ ($\bigcirc, \times$) and $l = 1, 3$ ($\square, +$) change their order for odd and even j. The broken and dotted curves show the variation of the semiclassical band centre and band boundaries.

The semiclassical and exact results are compared in table 3 and figure 6, where also the semiclassical band centre and band edges are shown. The overall trend of the quasienergy spectrum is reproduced semiclassically, in particular the approximate degeneracy (modulo $2\pi/s$), the formation of four-tuples in separate bands, the variation of the band centre as well as the increase of the band width. The levels inside a band are split into two pairs ($l = 0, 2$ and $l = 1, 3$) with roughly the same quasienergy differences. The position of these pairs inside a band interchange with odd/even band number j.

5. Tunnelling splittings of the quasienergies

Let us now look at the tunnelling splittings of the quasienergies for narrow bands well below the barrier, i.e. for parameters of the Mathieu equation (14) in the region $-2q < a \ll 2q$. Following [25], the splittings of the characteristic values a of the Mathieu equation are approximated by expanding α–ϕ in the neighbourhood of the band centre (29). The half width of the band j is approximately given by

$$\Delta_j = \left.\frac{\mathrm{d}(\alpha-\phi)}{\mathrm{d}a}\right|^{-1}_{\overline{a_j}} \mathrm{e}^{-\pi\overline{\epsilon_j}} \tag{39}$$

with

$$\left.\frac{\mathrm{d}(\alpha-\phi)}{\mathrm{d}a}\right|^{-1}_{\overline{a_j}} = \frac{s\pi\sqrt{q}}{K(k)} \tag{40}$$

and $\overline{\epsilon_j} = \epsilon(\overline{a_j})$ (note that $-1 \leqslant f_l \leqslant 1$). Using again the expansions for the elliptic integrals [26], the phase integral α over the well and the tunnelling integral are approximately given by

$$\alpha \approx \frac{2\pi}{s}\sqrt{q}k^2 \tag{41}$$

$$\pi\overline{\epsilon_j} \approx \frac{8}{s}\sqrt{q}\left[1 - \frac{k^2}{2}\ln\left(\frac{4}{k}\right) - \frac{k^2}{4}\right] \tag{42}$$

and the splitting of the a-values in band j can be written (using (34)) as

$$\Delta_j \approx \frac{s^2}{\pi}2^{4(j+1/2)}\frac{\mathrm{e}^{j+\frac{1}{2}-\frac{8}{s}\sqrt{q}}}{(j+\frac{1}{2})^{j+1/2}}\left(\frac{2}{s}\sqrt{q}\right)^{j+\frac{3}{2}}. \tag{43}$$

The individual characteristic values inside band j are then given by

$$a_{j,l} = \overline{a_j} - (-1)^j\Delta_j f_l \tag{44}$$

with an average value of $\overline{a_j}$.

Semiclassically, the $\hbar$-dependence of the tunnelling splitting is of interest. With $\sqrt{q} = A/16\hbar$ in (43), the combined polynomial-exponential dependence can be written as

$$\Delta_j \sim \hbar^{-(j+3/2)}\mathrm{e}^{-\delta/\hbar} \tag{45}$$

with $\delta = A/2s$. The approximate quasienergies in band j—taken modulo $\hbar\omega/s$—given in (19) are

$$\varepsilon'_{j,l} \approx \overline{\varepsilon'_j} + \Delta\varepsilon'_j f_l \tag{46}$$

where $\overline{\varepsilon'_j}$ is defined in (35), and

$$\Delta\varepsilon'_j = -\hbar\omega_0\frac{8\hbar}{sA}(-1)^j\Delta_j. \tag{47}$$

The splitting of the quasiangles (5)—modulo $2\pi/s$—can then be written equivalently as

$$\theta'_{j,l} = \overline{\theta'_j} + \Delta\theta'_j f_l \tag{48}$$

with

$$\Delta\theta'_j = -\omega_0 T\frac{8\hbar}{sA}(-1)^j\Delta_j \tag{49}$$

which shows—up to the additional factor of $\overline{h}$—the same $\overline{h}$-scaling as (45):

$$(\Delta\theta)_j \sim \overline{h}^{-(j+1/2)}\mathrm{e}^{-\delta/\overline{h}}. \tag{50}$$

Two different origins of the splittings should be distinguished.

(i) The tunnelling integral, $\pi\overline{\epsilon_j}$, resulting from a classically forbidden transition between the classical stability islands determines the overall splitting of the band, i.e. the band width.

(ii) The quasienergies of individual states of the s-tuple in each band are split by the terms $\overline{h}\omega rl/s (l = 0, \ldots, s-1)$, which disappear when taken modulo $\overline{h}\omega/s$, as well as by the f_l-terms (21). These splittings arise from the matching conditions for the phases and are closely related to the symmetry properties of the states.

Semiclassical tunnelling through classically forbidden regions in phase space for two-dimensional time-independent systems has been discussed by Wilkinson [28], who conjectured a scaling of the energy splittings as

$$\Delta E - \overline{h}^{-3/2}\mathrm{e}^{-S/\overline{h}} \tag{51}$$

where S is a constant, in agreement with the scaling (45) for the lowest band. This scaling law is, however, based on the existence of the classical tori, i.e. on the approximate integrability of the system. Deviations from this simple scaling law for strongly distorted systems are likely, where the classical separatrix develops into a chaotic layer (see [14] for a recent study).

6. Wavefunctions and wavepacket dynamics

In this section we will describe the semiclassical wavefunction supported by a group of flux tubes in more detail, as well as the symmetry and localization properties and the suppression of tunnelling.

6.1. Tunnelling between flux tubes

The semiclassical (EBK) quantization of quasienergy states [17, 21, 22] provides semiclassical wavefunctions $v(t)$, which are supported by the single sT-periodic flux tube following the periodic orbit at its centre. Defining segments $v_j^{(\nu)}(t) = v_j(t + \nu T)$, $\nu = 0, \ldots, s-1$, of length T, we can construct a s-fold centre of flux tubes in the period $0 \leqslant t \leqslant T$ (see figure 2 in paper I for an illustration).

Neglecting tunnelling, it was shown in paper I that the primitive semiclassical quasienergy states for the island chain can be built up from this flux cable. The quasienergy wavefunction is given by

$$\Psi_{j,l,n_2}(t) = \mathrm{e}^{-\mathrm{i}\varepsilon_{j,l,n_2}t/\overline{h}}u_{j,l,n_2}(t) \approx \mathrm{e}^{-\mathrm{i}\overline{\varepsilon_j}t/\overline{h}}u_{j,l,n_2}(t) \tag{52}$$

where $\overline{\varepsilon_j'}$ is defined in (35) (the term $\overline{h}\omega\mu_1 r/4s$ is missing in equation (62) in paper I). The T-periodic functions $u_{j,l,n_2}(t)$ can be expressed as

$$u_{j,l,n_2}(t) = \left(\sum_{\nu=0}^{s-1} v_j^{(\nu)}(t)\mathrm{e}^{\mathrm{i}2\pi\nu lr/s}\right)\mathrm{e}^{\mathrm{i}(lr/s+n_2)\omega t}. \tag{53}$$

At the stroboscopic times $t_n = nT$, we find in particular

$$u_{j,l,n_2}(n) = \left(\sum_{\nu=0}^{s-1} v_j^{(\nu+n)}(0)\mathrm{e}^{\mathrm{i}2\pi\nu lr/s}\right)\mathrm{e}^{\mathrm{i}(lr/s+n_2)2\pi n} \tag{54}$$

with $v_j^{(\nu)}(nT) = v_j^{(\nu+n)}(0)$. By construction, there are only s different terms $v_j^{(0)}, \ldots, v_j^{(s-1)}$.

This does not depend on n_2, so that we can drop this index. We will simplify the notation even more by also dropping—for the moment—the band index j. Introducing the abbreviations $u_1 = u_l(0)$, $v^{(\nu)} = v^{(\nu)}(0)$ and $\sigma = \mathrm{e}^{\mathrm{i}2\pi r/s}$, (54) reduces to

$$u_l = \sum_{\nu=0}^{s-1} \sigma^{\nu l} v^{(\nu)} \tag{55}$$

which represents the quasienergy functions at the stroboscopic time as a linear combination of the semiclassical flux tube functions. It is of interest that the coefficient matrix does *not* depend on the band number j. (As it stands, the transformation (55) from the single flux tube states to the quasienergy states is not norm conserving; this can be achieved, however, by multiplication with the s-root of the determinant of the transformation matrix.)

For the simple case of a two-island chain $r : s = 1 : 2$ we have $\sigma = -1$ and (54) reads

$$\begin{pmatrix} u_0 \\ u_1 \end{pmatrix} = \begin{pmatrix} 1 & 1 \\ 1 & -1 \end{pmatrix} \begin{pmatrix} v^{(0)} \\ v^{(1)} \end{pmatrix}. \tag{56}$$

First we observe that the state u_0 is symmetric in $v^{(0)}$ and $v^{(1)}$, whereas u_1 is antisymmetric. Inverting (56)

$$\begin{pmatrix} v^{(0)} \\ v^{(1)} \end{pmatrix} = \tfrac{1}{2} \begin{pmatrix} 1 & -1 \\ 1 & 1 \end{pmatrix} \begin{pmatrix} u_0 \\ u_1 \end{pmatrix} \tag{57}$$

we see that states $v^{(\nu)}$, which are localized on a single island, can be constructed by subtracting and adding the quasienergy states. These facts are, of course, well known from tunnelling in a symmetric double-well potential.

Somewhat more interesting is the case of the $1 : 3$ resonance considered numerically in the preceding sections. The three functions $v^{(\nu)}$ localize on the three islands in the classical Poincaré section in figure 1. With $\sigma = \mathrm{e}^{\mathrm{i}2\pi/3}$, the transformation is

$$\begin{pmatrix} u_0 \\ u_1 \\ u_3 \end{pmatrix} = \begin{pmatrix} 1 & 1 & 1 \\ 1 & \sigma & \sigma^* \\ 1 & \sigma^* & \sigma \end{pmatrix} \begin{pmatrix} v^{(0)} \\ v^{(1)} \\ v^{(2)} \end{pmatrix}. \tag{58}$$

The state u_0 is symmetric in the $v^{(\nu)}$ and u_1, u_2 transform into each other by interchanging any pair of the $v^{(\nu)}$ up to a factor σ or σ^*. In terms of the C_3 symmetry, u_0 is the A-state and u_1, u_2 are the E-states (compare also with the discussion of a related semiclassical quantization of the three-fold restriction rotation in [29, 23]). In fact, the matrix in (58) agrees with the character table of this group. This holds also for the transformation (55) in general, which is related to the C_s point group.

Inverting (58), we obtain

$$\begin{pmatrix} v^{(0)} \\ v^{(1)} \\ v^{(2)} \end{pmatrix} = -\frac{1}{(1-\sigma)^2} \begin{pmatrix} -(1+\sigma^*) & \sigma & \sigma \\ \sigma & 1 & -(1+\sigma) \\ \sigma & -(1+\sigma) & 1 \end{pmatrix} \begin{pmatrix} u_0 \\ u_1 \\ u_2 \end{pmatrix} \tag{59}$$

which can be used to construct quantum states, which localize on a classical flux tube $v^{(\nu)}$ initially and follow the classical orbit $v^{(\nu+1)}$, $v^{(\nu+2)}$, $v^{(\nu+3)} = v^{(\nu)}$. In addition, the wavefunction Ψ picks up a phase factor $\mathrm{e}^{-\mathrm{i}\overline{\theta}'_j}$ at each period, where $\overline{\theta}'_j = \overline{\varepsilon}'_j T/\hbar$ is the quasiangle. Very clearly, the wavepacket will return to its initial island localization at times $3nT$.

This is, however, a simplified picture, because it neglects tunnelling. For example, if one starts a wavepacket constructed from a superposition of the three semiclassical quasienergy states $l = 0, 1, 2$ *including* the splitting—or, even more ambitious, the corresponding *exact* quantum states—the wavefunction will tunnel into the classically forbidden tubes of the

flux cable. On can gain some insight into this process by means of the narrow band approximation of the preceding section. Starting a wavepacket localized on island ν in band j initially (we still suppress the band index in the equations):

$$\Psi_\nu(0) = v^{(\nu)} = \sum_{l=0,1,2} d_{\nu l} u_l \tag{60}$$

with coefficients $d_{\nu,l}$ given in (59), we have at stroboscopic times $3nT$

$$\Psi_\nu(3nT) = \sum_{l=0,1,2} d_{\nu l} u_l \mathrm{e}^{\mathrm{i}\theta_l' 3n} \tag{61}$$

$$= \sum_{\nu'} f_{\nu\nu'}(3n) v^{(\nu')}. \tag{62}$$

The time-dependent probability amplitudes

$$f_{\nu\nu'}(3n) = \sum_{l=0,1,2} d_{\nu l} \sigma^{\nu' l} \mathrm{e}^{-\mathrm{i}\theta_l' 3n} \tag{63}$$

$$\approx \mathrm{e}^{-\mathrm{i}\bar{\theta}' 3n} \sum_{l=0,1,2} d_{\nu l} \sigma^{\nu' l} \mathrm{e}^{-\mathrm{i}\Delta\theta' f_l 3n} \tag{64}$$

(with $f_{\nu'\nu}(0) = \delta_{\nu\nu'}$) show a quasiperiodic tunnelling oscillation between the flux tubes with frequencies

$$\omega_{l'l} \sim |f_l' - f_l| = \left| 2 \sin \frac{\pi}{s} \left(l' + l + \frac{\mu}{2} \right) \cos \frac{\pi}{s} (l' - l) \right|. \tag{65}$$

Within the narrow band approximation (48), (49), this oscillation is strictly periodic if the ratio of two of the f_l is rational.

6.2. Degeneracies and suppression of tunnelling

In contrast to the energy eigenvalues for a one-dimensional double-well potential, the quasienergies can be degenerate. In the present context, this is easily achieved by varying the value of $\bar{h}$, keeping thus the underlying classical dynamics unchanged. In view of section 3, this can be done, for example, in an experiment by varying the frequency ω. From (17) we see that the (quasi) Maslov index $\nu/4$ is changed and two of the factors f_l in (21) or (65) can become degenerate. It might be helpful to illustrate this by the complex quantities $\mathrm{e}^{\mathrm{i}2\pi(l+\mu/4)/s}$, the roots of $z^s = \mathrm{e}^{\mathrm{i}\pi\mu/2}$ (f_l = real z), which are the n vertices of a regular polygon, rotated by an angle $\pi\mu/2$, which depends on $\bar{h}$.

The condition for such a degeneracy of states l and l' is

$$\frac{\mu}{2} = sN - l - l' \qquad N = 1, 2, \ldots \tag{66}$$

i.e. whenever $\mu/2$ is equal to an integer, pairs of the f_l—and hence semiclassical quasienergies ε_l'—are degenerate. Such a degeneracy occurs simultaneously in all bands j (note that this results from the semiclassical approximation, but is *not* a consequence of the narrow band approximation).

As an example, in figure 7 the characteristic value $a_{j,l}$ of the Mathieu equation (14) (i.e. the quasienergies (19) up to a linear transformation) are plotted as a function of the (scaled) $\bar{h}$ for the 1 : 3 resonance bands. The curves show a steep increase up to the separatrix value (which decreases with $\bar{h}$ because of $a_{\mathrm{sep}} = 2q = (A/4\bar{h})^2$) followed by a widening of the bands, where the three substates oscillate regularly undergoing repeated degeneracies in all bands. For even larger values of $\bar{h}$ the bands approach each other and the substates form a regular net, where the interband-crossings are small, but, still avoided.

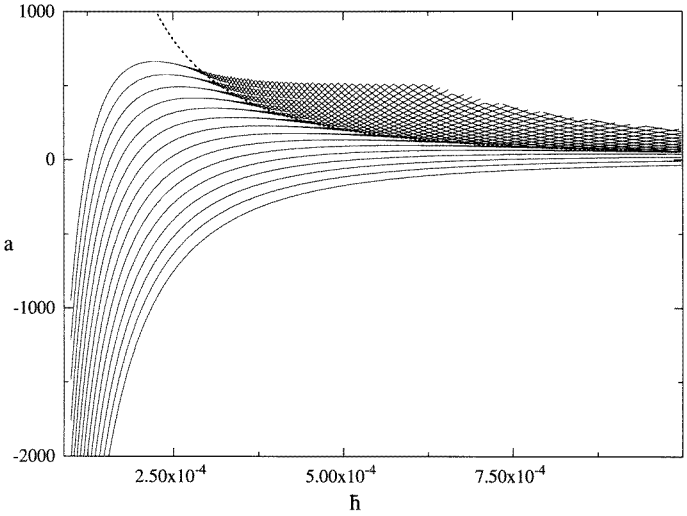

Figure 7. The characteristic Mathieu values $a_{j,l}$ show sequential degeneracies as a function of the scaled values of $\bar{h}$ simultaneously in all bands. Also shown in the separatrix value $a_{\text{sep}} \sim \bar{h}^{-2}$.

In case of a degeneracy of substates l and l', one can construct a wavefunction, which is localized on any pair of flux tubes. The tunnelling to the third flux tube is suppressed, i.e. one of the islands is not populated at times $3nT$. Such an anti-localization on tube ν can be achieved by taking a linear combination of the quasienergy states

$$\Psi(0) = \sum_{\nu'=0,1,2} c_{\nu'} u_{\nu'} \tag{67}$$

with $c_{l''} = 0$ (l and l' degenerate, $l \neq l'' \neq l'$) and

$$c_{l'} = -c_l \qquad \text{for } \nu = 0 \tag{68}$$

$$c_{l'} = -\sigma c_l \qquad \text{or} \qquad c_{l'} = -\sigma^* c_l \qquad \text{for } \nu = 1, 2. \tag{69}$$

An initial state (67)–(69) shows a time variation at $t = 3nT$ as

$$\Psi(3n) = \sum_{\nu'=0,1,2} c_{\nu'} u_{\nu'} \mathrm{e}^{\mathrm{i}\theta'_{\nu'} 3n} \tag{70}$$

$$= c_{l'} u_{l'} + c_l u_l) \mathrm{e}^{\mathrm{i}\theta'_l 3n} = \Psi(0) \mathrm{e}^{\mathrm{i}\theta'_l 3n} \tag{71}$$

i.e. the probability distribution remains constant.

7. Concluding remarks

We have analysed the splitting of the quasienergy states in periodically driven quantum systems due to tunnelling between classical resonance flux tubes in continuation of previous work on semiclassical EBK quantization [17, 22]. The resulting semiclassical approximation provides a simple method for computing the quasienergies and their splittings from a few classical data by means of phase integrals over the flux tube and the dynamical barrier. Numerical applications to a driven quartic oscillator demonstrated the applicability of this approximation, which may be useful for more realistic systems because very small tunnelling splittings are difficult to compute quantum mechanically. Moreover, the semiclassical

analysis provides a useful skeleton for the overall organization of the quasienergy spectrum, which can be labelled by semiclassical quantum numbers.

At the present time, we are not aware of experimental data of quantum tunnelling splittings between classical flux tubes, which allow a direct quantitative application of the present analysis. There is, however, a strong experimental effort to control and stabilize states of atomic or molecular systems in time periodic fields, e.g. strong laser fields. In particular, it should be possible to populate resonance island states, e.g. by controlling the time variation of suitable system parameters. We hope that our prediction of tunnelling between flux tubes will be experimentally observed in the future.

In closing, we would like to point out that there are also some open problems in the theoretical understanding of these tunnelling processes, because the present analysis is developed and tested for a system, which is almost regular. It should be of some interest to study the influence of increasing chaoticity on the splittings for tunnelling transitions through the chaotic separatrix layer. Work along these lines is in progress.

Acknowledgment

This work has been supported by the Deutsche Forschungsgemeinschaft (SPP 'Zeitabhängige Phänomene und Methoden in Quantensystemen der Physik und Chemie')

References

[1] Davis M J and Heller E J 1981 *J. Chem. Phys.* **75** 246
[2] Lin W A and Ballentine L E 1990 *Phys. Rev. Lett.* **65** 2927
[3] Lin W A and Ballentine L E 1992 *Phys. Rev.* A **45** 3637
[4] Peres A 1991 *Phys. Rev. Lett.* **67** 158
[5] Plata J and Gomez Llorente J M 1992 *J. Phys. A: Math. Gen.* **25** L303
[6] Grossmann F, Jung P, Dittrich T and Hänggi P 1991 *Phys. Rev. Lett.* **67** 516
Grossmann F, Jung P, Dittrich T and Hänggi P 1991 *Z. Phys.* B **84** 315
[7] Grossmann F, Dittrich T and Hänggi P 1991 *Physica* **175B** 293
[8] Grossmann F, Dittrich T, Jung P and Hänggi P 1993 *J. Stat. Phys.* **70** 229
[9] Hänggi P, Utermann R and Dittrich T 1994 *Physica* **194–6B** 1013
[10] Utermann R, Dittrich T and Hänggi P 1994 *Phys. Rev.* E **49** 273
[11] Grobe R and Haake F 1987 *Z. Phys.* B **68** 503
[12] Casati G, Graham R, Guarneri I and Izrailev F M 1994 *Phys. Lett.* A **190** 159
[13] Averbuckh V, Moiseyev N, Mirbach B and Korsch H J 1995 *Z. Phys.* D **35** 247
[14] Roncaglia R, Bonci L, Izrailev F M, West B J and Grigolini P 1994 *Phys. Rev. Lett.* **73** 802
[15] Lebœuf P and Mouchet A 1994 *Phys. Rev. Lett.* **73** 1360
[16] Leyvraz F and Ullmo D 1996 *J. Phys. A: Math. Gen.* **29** 2529
[17] Mirbach B and Korsch H J 1994 *J. Phys. A: Math. Gen.* **27** 6579
[18] Thylwe K-E 1993 *J. Sound Vib.* **161** 203
[19] Abraham R and Marsden J E 1978 *Foundations of Mechanics* (Reading, MA: Benjamin)
[20] Howland J S 1989 *Ann. Inst. Henri Poincaré Phys. Theor.* **50** 309
Howland J S 1989 *Ann. Inst. Henri Poincaré Phys. Theor.* **50** 325
[21] Breuer H P and Holthaus M 1991 *Ann. Phys., NY* **211** 249
[22] Bensch F, Korsch H J, Mirbach B and Ben-Tal N 1992 *J. Phys. A: Math. Gen.* **25** 6761
[23] Child M S 1991 *Semiclassical Mechanics with Molecular Applications* (Oxford: Oxford University Press)
[24] Sirko L and Kock P M 1995 *Appl. Phys.* B **60** S195
[25] Connor J N L, Uzer T, Marcus R A and Smith A D 1984 *J. Chem. Phys.* **80** 5095
[26] Lebedew N N 1973 *Spezielle Funktionen und ihre Anwendungen* (Berlin: Wissenschaftsverlag)
[27] Thylwe K-E and Bensch F 1994 *J. Phys. B: At. Mol. Opt. Phys.* **27** 5673
Thylwe K-E and Bensch F 1994 *J. Phys. B: At. Mol. Opt. Phys.* **27** 7475
[28] Wilkinson M 1987 *J. Phys. A: Math. Gen.* **20** 635
[29] Child M S 1974 *J. Molec. Spec.* **53** 280